Effects of Tidal Shallowing and Deepening on Phytoplankton Production Dynamics: A Modeling Study

Lisa V. Lucas* and James E. Cloern

U.S. Geological Survey, 345 Middlefield Road, MS 496, Menlo Park, California 94025

ABSTRACT: Processes influencing estuarine phytoplankton growth occur over a range of time scales, but many conceptual and numerical models of estuarine phytoplankton production dynamics neglect mechanisms occurring on the shorter (e.g., intratidal) time scales. We used a numerical model to explore the influence of short time-scale variability in phytoplankton sources and sinks on long-term growth in an idealized water column that shallows and deepens with the semidiurnal tide. Model results show that tidal fluctuations in water surface elevation can determine whether long-term phytoplankton growth is positive or negative. Hourly-scale interactions influencing weekly-scale to monthly-scale phytoplankton dynamics include intensification of the depth-averaged benthic grazing effect by water column shallowing and enhancement of water column photosynthesis when solar noon coincides with low tide. Photosynthesis and benthic consumption may modulate over biweekly time scales due to spring-neap fluctuations in tidal range and the 15-d cycle of solar noon-low tide phasing. If tidal range is a large fraction of mean water depth, then tidal shallowing and deepening may significantly influence net phytoplankton growth. In such a case, models or estimates of long-term phytoplankton production dynamics that neglect water surface fluctuations may overestimate or underestimate net growth and could even predict the wrong sign associated with net growth rate.

Introduction

Most paradigms for explaining the production dynamics of phytoplankton in estuaries do not consider the effects of tidal variability. Estuarine phytoplankton growth is often described instead as a function of seasonal variations in irradiance, grazing, and inputs of heat, nutrients, and freshwater, as well as daily to weekly fluctuations in tidal energy, vertical mixing, density stratification, turbidity, and horizontal transport (see Cloern 1996). Episodic events such as storms and associated increases in vertical mixing, sediment resuspension, horizontal transport, or nutrient input have also been shown to cause abrupt changes in phytoplankton biomass (Huzzey et al. 1990). Shorter (i.e., hourly) time-scale periodic processes have been explored less frequently as mechanisms potentially governing long-term bloom dynamics. Periodic short time-scale mechanisms include oscillatory tidal advection of phytoplankton biomass across gradients of net phytoplankton growth (Lucas et al. 1999b), vertical displacement of chlorophyll gradients by internal waves, diel cycles of vertical migration, chlorophyll a (chl a) synthesis and cell division, and tidal or periodic wind-driven resuspension of benthic microalgae (Cloern et al. 1989).

We explore another high-frequency mechanism of variability in estuaries: hourly-scale fluctuations in the phytoplankton source-sink balance due to

tidal shallowing and deepening of the water column (Lucas et al. 1999a). Estuarine phytoplankton population growth depends in part on local sources and sinks: light-driven photosynthesis, algal respiration, and consumption by grazers. (We use the term population to connote bulk phytoplankton biomass estimated as carbon concentration, as opposed to cell number or density.) Phytoplankton population growth is also influenced by horizontal transport (Lucas et al. 1999b), but we focus here on the idealized case of a horizontally homogeneous water column where horizontal variability and net horizontal transport are assumed to be zero. Phytoplankton population growth in this idealized system is governed completely by the local balance of biomass sources and sinks. If we further assume this water column is vertically well-mixed, then we can describe phytoplankton production dynamics with depth-averaged growth and loss.

Some phytoplankton sources and sinks vary with vertical position in the water column, so depth-averaged growth and loss rates are functions of water column height, H. For example, photosynthetically active radiation decreases exponentially with depth, so phytoplankton in a well-mixed shallow water column, on average, encounter more light and photosynthesize more rapidly than in a well-mixed deep water column (i.e., the phytoplankton source varies inversely with H). An important sink for phytoplankton biomass is benthic grazing, which is localized at the sediment-water interface but has an effect distributed over the full water

* Corresponding author; tele: 650/329-4588; fax: 650/329-4327; e-mail: llucas@usgs.gov.

column when it is vertically mixed. This distributed effect is strongest in shallow water columns, so the benthic sink varies inversely with H. Since the phytoplankton source-sink terms vary with H, they vary over short time scales in a tidal water column. We examine this time-dependent relationship of local phytoplankton source and sinks with H and explore the hypothesis that tidal oscillations of H about a mean height, $\overline{H}$, can result in long-term phytoplankton growth different from growth in a non-tidal system having the same $\overline{H}$.

We employ a simple numerical model to study the sensitivity of estuarine phytoplankton production dynamics to tidally oscillating water column height. Our zero-dimensional model (Zero-D) accounts only for changing local dynamics (i.e., horizontal variability and transport are neglected). The Zero-D model is depth-averaged and therefore built on the assumption that the water column is energetic and vertically well mixed (i.e., the vertical phytoplankton distribution is uniform). This approach of using a simple model to simulate dynamics under idealized conditions does not capture all processes governing phytoplankton growth in real estuaries. This approach does allow us to isolate a targeted set of processes for illustrating a central point: hourly-scale fluctuations in estuaries can, under some conditions, have a large impact on the population dynamics of phytoplankton at the longer (weekly, monthly) time scales characteristic of many sampling programs. Using results of model simulations, we ask if tidal shallowing and deepening alone can result in significantly different phytoplankton dynamics from an otherwise identical non-tidal (lake-like) system, if the relationship between phytoplankton population growth and tidal range is monotonic, what processes govern the relationship between phytoplankton population growth and tidal range, under what conditions is phytoplankton population growth especially sensitive to tidal range, and should estuarine phytoplankton ecologists and ecosystem modelers incorporate tidal time-scale processes into their conceptual and numerical models?

Methods

The local source and sinks for a vertically well-mixed phytoplankton population can be combined into an effective growth rate, μ_{eff}, which is derived by averaging a vertical phytoplankton evolution equation (including terms for vertical turbulent diffusion, sinking, and net population growth rate) over the total depth, H. A no-flux boundary condition is applied at the surface, and the total bottom flux is limited to an advective benthic grazing

flux (Koseff et al. 1993). The resulting expression for μ_{eff} is (Lucas et al. 1999a):

$$\mu_{\text{eff}}(t) = \mu_{\text{pelagic}}(t) + \mu_{\text{benthic}}(t) \qquad (1)$$

where μ_{pelagic} includes pelagic processes (carbon assimilation, chlorophyll synthesis, algal respiration, zooplankton grazing), and $\mu_{\text{benthic}} = -\alpha/H(t)$ is the depth-averaged benthic grazing effect (α is benthic grazing rate in m d^{-1}). The net pelagic phytoplankton source, μ_{pelagic}, is calculated using

$$\mu_{\text{pelagic}}(t) = P(t)[\text{chl:C}] - \text{resp}(t) - ZP \qquad (2)$$

where P is depth-averaged photosynthetic carbon assimilation rate per unit chl a; [chl:C] is the ratio of cellular chl a to carbon in phytoplankton (assumed constant here); resp, the respiration loss rate, is the sum of a constant basal rate and a component proportional to growth rate (see Cloern et al. 1995); and ZP is the zooplankton grazing rate (assumed constant at 0.1 d^{-1}, characteristic of South San Francisco Bay; Cloern 1982). P is calculated as:

$$P(t) = \frac{1}{H(t)} \int_{-H(t)}^{0} p(z, t) \, dz \qquad (3)$$

where:

$$p(z, t) = p_{\text{max}}[1 - \exp(-I(z, t)a/p_{\text{max}})] \qquad (4)$$

Equation 4 describes instantaneous photosynthesis, p, at depth z as a function of physiological parameters a and p_{max} and of light, I(z, t) (determined by solar radiation at the water surface, I(0), photoperiod, D, and abiotic attenuation coefficient, k_t; see Cloern et al. 1995). Self-shading is incorporated by adding to k_t a biotic component of light attenuation calculated as the chlorophyll-specific attenuation (0.016 m^2 mg chl a^1; Bannister 1974) multiplied by the chlorophyll biomass [mg chl a m^{-3}]. The integral in Eq. 3 is calculated with a series approximation similar to that of Platt et al. (1991). Here, we assume that nutrients are not limiting.

The Zero-D model calculates μ_{eff} as a time-dependent function of the diurnal light cycle and tidally oscillating water column height. Surface irradiance during the day is a sinusoidal function, reaching a maximum at solar noon. H(t) is calculated as:

$$H(t) = \overline{H} + 0.5\Delta H \sin(2\pi t/\tau) \qquad (5)$$

where $\overline{H}$ is mean water column height, ΔH is tidal range (H at high tide minus H at low tide), t is time, and τ is tidal period (0.5175 d for a semidiurnal tide).

Time-varying depth-averaged phytoplankton biomass B is calculated as:

TABLE 1. Physiological and environmental parameters and calculated variables. Parameters are representative of South San Francisco Bay in early spring.

Variable/Parameter	Units	Value	Description	Comments/Source
a	mg C mg chl a^{-1} h^{-1} (μmol quanta m^{-2} s^{-1})$^{-1}$	0.031	Photosynthetic efficiency at low irradiance	Lucas et al. (1999a)
B(t)	mg C m^{-3}		Depth-averaged phytoplankton biomass	
[chl:C]	mg chl a mg C^{-1}	0.030	Phytoplankton cellular ratio of chl a to carbon	Cloern et al. (1995)
D	h	12	Photoperiod	Lucas et al. (1999a)
H(t)	m		Water column height	
$\overline{H}$	m	0.5–10.0	Mean water column height	
I(z, t)	μmol quanta m^{-2} s^{-1}		Instantaneous irradiance at depth z	
I(0)	mol quanta m^{-2} d^{-1}	28	Total daily surface irradiance (quantum flux, photosynthetically active radiation)	Lucas et al. (1999a)
I$_{surf}$	μmol quanta m^{-2} s^{-1}		Instantaneous surface irradiance	
k$_t$	m^{-1}	0.4–15	Abiotic light attenuation coefficient	
k$_t^*$	—		Dimensionless turbidity	
p(z, t)	mg C mg chl a^{-1} h^{-1}		Instantaneous rate of photosynthesis at depth z	
p$_{max}$	mg C mg chl a^{-1} h^{-1}	8.5	Maximum instantaneous photosynthetic rate	Lucas et al. (1999a)
P(t)	mg C mg chl a^{-1} h^{-1}		Instantaneous depth-averaged rate of photosynthesis	
resp	d^{-1}	0.018 ± 0.18 ($\mu_{pelagic}$ + ZP)	Phytoplankton rate of loss to respiration	Cloern et al. (1995)
t	d		Time	
z	m		Depth	
ZP	d^{-1}	0.1	Zooplankton grazing rate	Cloern (1982)
α	md^{-1}	0–7	Benthic grazing rate	
α*	—		Dimensionless benthic grazing rate	
α$_x$	md^{-1}		Critical benthic grazing rate	
α$_x^*$	—		Dimensionless critical benthic grazing rate	
ΔH	m	0–5	Tidal range	
ΔH*	—		Dimensionless tidal range	
$\mu_{benthic}$	d^{-1}		Depth-averaged benthic grazing effect	
μ_{eff}	d^{-1}		Phytoplankton effective growth rate	
$\mu_{pelagic}$	d^{-1}		Net pelagic phytoplankton source	
τ	h	12.42	Tidal period	

$$B(t + \Delta t) = B(t)\exp(\mu_{eff}\Delta t) \qquad (6)$$

where B grows if μ_{eff} is positive and decays if μ_{eff} is negative ($\Delta t = 0.01$ d is the simulation time step).

We used the Zero-D model to calculate time series of B for different combinations of $\overline{H}$, ΔH, turbidity (k$_t$), and benthic grazing rate (α). For all simulations, I(0), D, p$_{max}$, a, α, and ZP were held constant and based on values typical of South San Francisco Bay in the spring (see Table 1 for parameter values and ranges). $\overline{H}$ and ΔH were held constant, except where spring-neap variability in tidal range was considered. For that case, a time series of H(t) was calculated with a two-dimensional depth-averaged hydrodynamic model of South San Francisco Bay and input to the Zero-D model (Casulli 1990a,b; Cheng et al. 1993; Gross et al. 1999).

We used an iterative version of the Zero-D model (Zero-DI) to examine sensitivity of long-term phytoplankton growth to tidal shallowing and deepening over a broad range of conditions. For a given $\overline{H}$, ΔH, and k$_t$, Zero-DI iteratively determines α$_x$, the critical benthic grazing rate (Lucas et al. 1999a), which makes average net phytoplankton growth (μ_{eff}) over time equal to zero. α$_x$ represents a growth-decay threshold: if α < α$_x$ then phytoplankton biomass grows, and if α > α$_x$ then phytoplankton biomass decreases. α$_x$ simplifies the multi-parameter problem of bloom development, since it collapses two variables (B and α) into one. For a set I(0), D, p$_{max}$, a, and ZP, we used the Zero-DI model to determine α$_x$ for over 7,000 combinations of $\overline{H}$, ΔH, and k$_t$. Since μ_{eff} varies continuously in time due to tidal oscillations of H, the diurnal light cycle, and their relative phasing, we removed phasing bias by reporting α$_x$ as that α for which average μ_{eff} is zero over a 15-d simulation period (an even multiple of the semidiurnal tidal and day-night periods).

Results

CONSTANT TIDAL RANGE

Figure 1 shows specified time series of H and instantaneous surface irradiance (I$_{surf}$) as well as calculated phytoplankton biomass (B), pelagic net source ($\mu_{pelagic}$), and benthic sink ($\mu_{benthic}$) for a shallow, clear water column with strong benthic

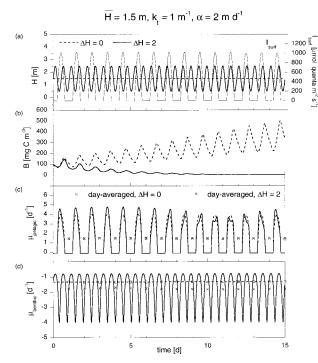$\overline{H} = 1.5$ m, $k_t = 1$ m^{-1}, $\alpha = 2$ m d^{-1}

Fig. 1.   Specified water column height and surface irradiance (a) and calculated phytoplankton biomass (b), pelagic net phytoplankton source (c), and benthic sink (d) for a shallow, clear water column with strong benthic grazing. Two tidal conditions are compared: $\Delta H = 0$ (non-oscillating water surface elevation) and $\Delta H = 2$ m (approximate tidal range of San Francisco Bay).

$\overline{H} = 1.5$ m, $k_t = 10$ m^{-1}, $\alpha = 0.2$ m d^{-1}
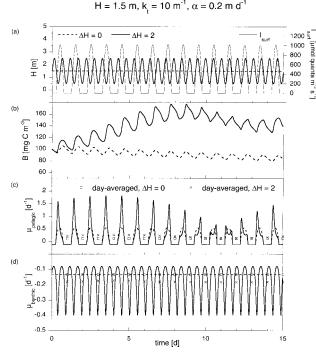

Fig. 2.   Specified water column height and surface irradiance (a) and calculated phytoplankton biomass (b), pelagic net phytoplankton source (c), and benthic sink (d) for a shallow, turbid water column with weak benthic grazing. Two tidal conditions are compared: $\Delta H = 0$ and $\Delta H = 2$ m.

grazing ($\overline{H} = 1.5$ m; $k_t = 1.0$ m^{-1}; $\alpha = 2.0$ m d^{-1}). We compared two tidal conditions: $\Delta H = 2$ m (approximate tidal range of San Francisco Bay) and $\Delta H = 0$ (non-oscillating water column height, e.g., a lake). The two tidal conditions yielded very different results: phytoplankton grew over time in the non-oscillating water column but decayed in the oscillating water column (Fig. 1b). Day-averaged and maximum daytime μ_{pelagic} were slightly higher for the oscillating tidal condition than for the nontidal condition (Fig. 1c) if solar noon coincided approximately with low tide (Fig. 1a; days 1–7). On days 10–13, solar noon occurred at or near high water (Fig. 1a), decreasing depth-averaged irradiance and μ_{pelagic} (Fig. 1c). Since μ_{pelagic} for non-zero ΔH was on average slightly higher than for zero ΔH, the decrease of B for $\Delta H = 2$ m (Fig. 1b) is explained by differences in μ_{benthic}. $|\mu_{\text{benthic}}|$ became very large during low tides, overriding any increase in μ_{pelagic} during low tides and causing an overall decrease in B (Fig. 1d). The specific loss rate to benthic grazing scales inversely with H, so benthic grazers filter a larger fraction of the total phytoplankton biomass during low tide than during high tide.

Figure 2 shows model results for a shallow water

column with conditions representing the inverse of the case in Fig. 1: turbid with weak benthic grazing ($\overline{H} = 1.5$ m; $k_t = 10.0$ m^{-1}; $\alpha = 0.2$ m d^{-1}). We compared two tidal conditions ($\Delta H = 0$ and 2 m), and B again followed two very different trajectories (Fig. 2b). However, for this case oscillating H resulted in overall positive phytoplankton growth, and constant $H = \overline{H}$ resulted in negative growth (inverse of the result shown in Fig. 1b). On days when solar noon coincided approximately with low tide (Fig. 2a; days 1–7), daily maximum μ_{pelagic} in the turbid oscillating water column more than doubled the μ_{pelagic} associated with zero ΔH, overwhelming the benthic loss rate since α was small (Fig. 2c,d). When solar noon occurred around high tide (Fig. 2a; days 10–13), photosynthesis was less than respiration plus grazing losses, resulting in a decrease in B (Fig. 2b).

In Fig. 3, a case is shown for which shallowing and deepening resulted in similar phytoplankton dynamics as for a non-oscillating water column. We show model results for a deep, clear water column with strong benthic grazing ($\overline{H} = 10.0$ m; $k_t = 1.0$ m^{-1}; $\alpha = 2.0$ m d^{-1}). B increased overall for both $\Delta H = 0$ and 2 m, and it attained the same final magnitude (Fig. 3b) because differences in μ_{pelagic} (Fig. 3c) and μ_{benthic} (Fig. 3d) over this range of
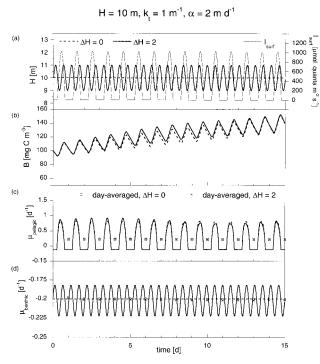
Fig. 3.   Specified water column height and surface irradiance (a) and calculated phytoplankton biomass (b), pelagic net phytoplankton source (c), and benthic sink (d) for a deep, clear water column with strong benthic grazing. Two tidal conditions are compared: $\Delta H = 0$ and $\Delta H = 2$ m.

ΔH were very small (order[0.01–0.1]) and compensated approximately for each other.

Figures 1 and 2 demonstrate that, under some conditions, phytoplankton dynamics are sensitive to tidal fluctuations in water column height. Figure 3 demonstrates that, under other sets of conditions, phytoplankton biomass will have the same growth trajectories for oscillating and non-oscillating H. The sensitivity of B(t) to ΔH appears to depend on benthic grazing rate, turbidity, and mean water column height. Can we generalize this information into a rule for identifying conditions when phytoplankton growth may be a strong function of tidal range? The dimensionless map of critical benthic grazing rate (α_x) in Fig. 4 is a two-dimensional representation of this multi-parameter problem. By employing α_x and non-dimensionalization techniques, we collapsed four independent variables (α, k_t, $\overline{H}$, and ΔH) and one dependent variable (B) into one plot relating the sensitivity of phytoplankton population growth to tidal range. Each symbol location in Fig. 4 represents a unique combination of k_t, $\overline{H}$, and ΔH for which the Zero-DI model determined that value of α where net phytoplankton growth is zero. The horizontal axis is dimensionless turbidity, $k_t^* = k_t \overline{H}$, and the vertical axis is dimensionless tidal range $\Delta H^* = \Delta H / \overline{H}$. Each symbol

type represents a specific range of dimensionless critical grazing rate $\alpha_x^* = \alpha_x \tau / \overline{H}$. For a particular combination of k_t, $\overline{H}$, and ΔH, α_x is the benthic grazing threshold dividing phytoplankton biomass increase and decrease. Figure 4 is a map of biomass equilibrium conditions (i.e., parameter combinations ensuring exactly zero growth). Figure 4 represents 7,350 combinations of k_t, $\overline{H}$, and ΔH, for which fixed values of I(0), D, p_{max}, a, and ZP were used (for different I(0), D, p_{max}, a, or ZP, a different α_x^*-ΔH^*-k_t^* plot would result).

The dimensionless α_x^* map in Fig. 4 is a binary indicator of phytoplankton biomass increase versus decrease: for a given k_t^* and ΔH^*, phytoplankton biomass will grow if $\alpha^* < \alpha_x^*$ and decline if $\alpha^* > \alpha_x^*$. The right side of Fig. 4 represents low water column irradiance (high turbidity and/or large total depth). For those conditions of strong light limitation, phytoplankton biomass can only increase if benthic grazing is weak (α_x^* is small). The left side of Fig. 4 represents high water column irradiance (low turbidity and/or shallow total depth). For water columns with high irradiance, phytoplankton biomass increases even in the presence of rapid benthic grazing (α_x^* is large).

The α_x^* map also identifies conditions under which phytoplankton production dynamics are sensitive to tidal range. It does not predict the magnitude of a bloom or the actual rate of biomass increase or decrease, but it indicates the relative rates of phytoplankton population growth for different combinations of k_t^* and ΔH^*. Where an iso-α_x^* line is vertical, one value of benthic grazing rate will ensure biomass equilibrium over that range of ΔH^* (net phytoplankton growth is insensitive to tidal oscillations). This is generally the case for small values of ΔH^*; the smaller the tidal range relative to mean water column height, the less sensitive phytoplankton growth is to water surface oscillations. This regime corresponds to the deep water column in Fig. 3. For that case, $k_t^* = 10$, $\alpha^* = 0.1035$, and $\Delta H^* = 0$ and 0.2 (see points labeled 3-R0 and 3-R2, respectively, in Fig. 4). Because $\alpha^* < \alpha_x^*$ (≈ 0.125), phytoplankton biomass increased over time (Fig. 3); because the α_x^* contours near points 3-R0 and 3-R2 are approximately vertical, there was almost no difference in growth for the two tidal conditions.

For larger values of ΔH^*, iso-α_x^* lines bend over, signifying a change in net phytoplankton growth with increasing dimensionless tidal range. In the low irradiance-low grazing regime (right side of Fig. 4), α_x^* contours bend to the right, indicating that, as tidal range increases, phytoplankton biomass can grow in the presence of increasingly stronger benthic grazing. This is due to the low
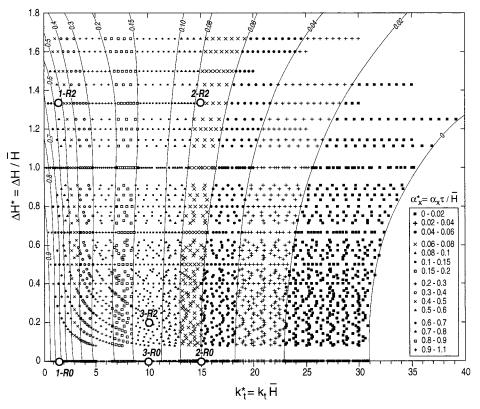
Fig. 4. Dimensionless map of phytoplankton biomass equilibrium conditions. Horizontal axis is dimensionless turbidity, vertical axis is dimensionless tidal range, and contours represent dimensionless critical benthic grazing rate. Points 1(2,3)-R0 and 1(2,3)-R2 correspond to the simulations shown in Fig. 1(2,3) for tidal range of 0 and 2 m, respectively.

tide periods provided by an oscillating water column which, on average, enhance water column irradiance and $\mu_{pelagic}$, an effect especially important in a turbid water column. In this regime α_x^* is small so enhancement of $\mu_{benthic}$ by water column shallowing is relatively unimportant. This regime corresponds to the high turbidity-low grazing case in Fig. 2. For that scenario, $k_t^* = 15$, $\alpha^* = 0.069$, and $\Delta H^* = 0$ and 1.33 (see points labeled 2-R0 and 2-R2, respectively, in Fig. 4). For the non-oscillating case ($\Delta H^* = 0$; point 2-R0), $\alpha_x^* \approx 0.06$; grazing exceeded its equilibrium threshold ($\alpha^* > \alpha_x^*$) and phytoplankton biomass decreased (Fig. 2). Because the $\alpha_x^* = 0.06$ contour bends to the right, the oscillating case ($\Delta H^* = 1.33$; point 2-R2) was associated with a higher dimensionless grazing threshold ($\alpha_x^* \approx 0.078$); grazing was less than its equilibrium threshold ($\alpha^* < \alpha_x^*$) and phytoplankton biomass increased (Fig. 2). For some conditions tidal oscillation of H causes a shift from one domain of Fig. 4 (with a particular α_x^*) into a different domain (with a different α_x^*).

In the high irradiance-high grazing regime (left side of Fig. 4), α_x^* contours bend to the left, indicating that, as tidal range increases, positive phytoplankton growth requires less and less benthic

consumption. Although the interaction of low tide with the diel light cycle on average enhances water column irradiance and $\mu_{pelagic}$, that effect is overwhelmed by the enhancement of $\mu_{benthic}$ by water column shallowing when benthic grazing rate is large. This regime corresponds to the low turbidity-high grazing case in Fig. 1. For that scenario, $k_t^* = 1.5$, $\alpha^* = 0.69$, and $\Delta H^* = 0$ and 1.33 (see points labeled 1-R0 and 1-R2, respectively, in Fig. 4). For the non-oscillating case ($\Delta H^* = 0$; point 1-R0), $\alpha_x^* \approx 0.75$; grazing was less than its equilibrium threshold ($\alpha^* < \alpha_x^*$) and phytoplankton biomass increased (Fig. 1). Because the $\alpha_x^* = 0.6–0.8$ contours bend to the left, the oscillating case ($\Delta H^* = 1.33$; point 1-R2) was associated with a lower dimensionless grazing threshold ($\alpha_x^* \approx 0.55$); grazing exceeded its equilibrium threshold ($\alpha^* > \alpha_x^*$), and phytoplankton biomass decreased (Fig. 1).

TIDAL RANGE VARYING OVER SPRING-NEAP CYCLE

The model results in Figs. 1–4 are based on the assumption that tidal range is constant over time. Although a necessary starting point for understanding bloom sensitivity to tidal range, that assumption does not necessarily hold in real estuaries. Tidal range fluctuates, in some cases signifi-
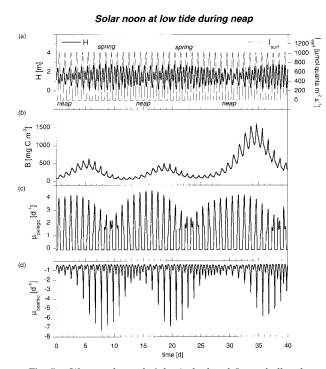
Solar noon at low tide during neap

Fig. 5. Water column height (calculated for a shallow location in South San Francisco Bay by a two-dimensional hydrodynamic model) and surface irradiance (a) and calculated phytoplankton biomass (b), pelagic net phytoplankton source (c), and benthic sink (d). Solar noon coincides with low water during neap tide.
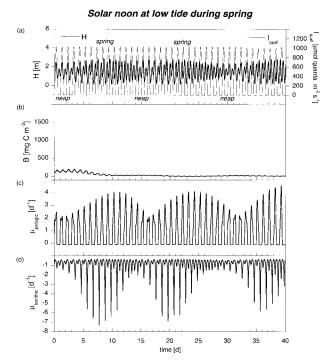
Solar noon at low tide during spring

Fig. 6. Water column height (calculated for a shallow location in South San Francisco Bay by a two-dimensional hydrodynamic model) and surface irradiance (a) and calculated phytoplankton biomass (b), pelagic net phytoplankton source (c), and benthic sink (d). Solar noon coincides with low water during spring tide.

cantly, over the fortnightly spring-neap cycle. Phytoplankton growth in some estuaries also appears to modulate with spring-neap fluctuations in tidal mixing, stratification, and sediment resuspension (Cloern 1996). If phytoplankton population growth is sensitive to tidal range, and if tidal range itself varies over the spring-neap cycle, then can weekly-scale variations in ΔH result in weekly-scale variations in phytoplankton growth, independent of fluctuations in stratification and sediment resuspension (Lucas et al. 1999a)?

Figure 5 shows model results for which realistic H(t) at a shallow location ($\overline{H} \approx 1.5$ m) in South San Francisco Bay was calculated by a two-dimensional hydrodynamic model. I(0), D, p_{max}, a, and ZP were the same in this case as for Figs. 1–4; $k_t = 2.0$ m^{-1} and $\alpha = 1.0$ m d^{-1}. $\mu_{pelagic}$ was highest during neap tide (Fig. 5c) because solar noon coincided with low water (Fig. 5a); during spring tide, $\mu_{pelagic}$ was minimized because solar noon coincided with high water. $|\mu_{benthic}|$ was maximal during spring tide, when H at lower low water was minimized (Fig. 5d). Because maximum $\mu_{pelagic}$ and minimum $|\mu_{benthic}|$ were approximately in phase (Fig. 5c,d), rapid growth was reinforced by slow grazing and phytoplankton population growth oc-

curred during neap tide (Fig. 5b). The inverse occurred during spring tide; since minimum $\mu_{pelagic}$ and maximum $|\mu_{benthic}|$ were approximately in phase (Fig. 5c,d), slow growth was compounded by rapid benthic grazing, and the phytoplankton population declined during spring tide (Fig. 5b). The biweekly scale phasing of $\mu_{pelagic}$ and $\mu_{benthic}$, which is controlled by hourly-scale interactions of water surface elevation with solar insolation and benthic grazing, can cause biweekly periodicity in phytoplankton net growth and biomass.

Figure 6 shows model results for a case identical to that in Fig. 5 except for a 6-h phase shift of solar noon relative to the semidiurnal tide. In this case $\mu_{pelagic}$ was minimal during neap tide (Fig. 6c) because solar noon coincided with high water (Fig. 6a); during spring tide $\mu_{pelagic}$ was maximized because solar noon coincided with low water. The time series of $\mu_{benthic}$ (Fig. 6d) is identical to the case in Fig. 5 ($|\mu_{benthic}|$ was maximum during spring tide). Because maximum $\mu_{pelagic}$ and maximum $|\mu_{benthic}|$ were approximately in phase, rapid growth during spring tide was countered by rapid grazing; similarly, during neap tide, when $|\mu_{benthic}|$ was minimized so was $\mu_{pelagic}$ (Fig. 6c,d). As a result, phytoplankton biomass in this scenario did not grow

overall (Fig. 6b). Comparison of Figs. 5 and 6 demonstrates that, all else being equal, the tidal-scale interaction of water surface elevation with solar insolation and benthic grazing can determine whether phytoplankton biomass increases or decreases over time scales of days to weeks.

Discussion

Tidal-scale fluctuations in water surface elevation can determine whether long-term phytoplankton growth is positive or negative, resulting in significantly different phytoplankton dynamics from an otherwise identical non-tidal system (Figs. 1 and 2). Because water column irradiance, photosynthesis, and the depth-averaged effect of benthic grazing are non-linear functions of depth, the time-averaged influence of oscillating H is not necessarily equivalent to the influence of a constant H equal to $\overline{H}$. Under some conditions, tidal water surface fluctuations do not have a significant impact on long-term phytoplankton growth (Fig. 3).

The relationship between phytoplankton population growth and tidal range is not monotonic. For a shallow clear water column with strong benthic grazing (Fig. 1), net phytoplankton growth decreases with increasing tidal range, but for a shallow turbid water column with weak benthic grazing (Fig. 2), net phytoplankton growth increases with increasing tidal range. This non-monotonic relationship between net growth and tidal range is evident in the map of bloom equilibrium conditions (Fig. 4): α_x^* contours bend to the right for large dimensionless turbidity and bend to the left for small dimensionless turbidity.

For given daily surface irradiance, photoperiod, zooplankton grazing rate, and photosynthesis-irradiance parameters, the relationship between phytoplankton population growth and tidal range depends on tidal range itself, turbidity, mean water column depth, and benthic grazing rate. If tidal range is small compared to mean water column height, then phytoplankton net growth is relatively insensitive to tidal range. If dimensionless tidal range is large, then phytoplankton growth may depend strongly on tidal range. The combination of turbidity and benthic grazing determines whether phytoplankton biomass increases or decreases with increasing tidal range. If water column irradiance is high and benthic grazing is strong, then phytoplankton growth decreases as tidal range increases. If water column irradiance is low and benthic grazing is weak, then phytoplankton growth increases as tidal range increases. Each combination of $I(0)$, D, p_{max}, a, and ZP produces a unique α_x^*-k_t^*-ΔH^* map, so these parameters determine the precise relationship between phytoplankton population growth and tidal range.
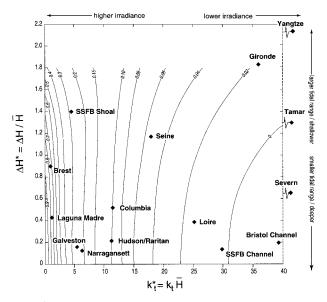

Fig. 7. Dimensionless map of phytoplankton biomass equilibrium conditions with superimposed points representing average conditions in real estuarine regions (Ministere de l'Environnement 1980; Joint and Pomroy 1981; Chen et al. 1982; Uncles 1982; Dyer 1984; Glover 1984; National Oceanic and Atmospheric Administration and United States Department of Commerce 1985; Stephens 1986; Uncles et al. 1986; Salomon 1988; Megard and Berman 1989; National Oceanic and Atmospheric Administration 1990; Monbet 1992; Eisma 1998; Lucas et al. 1999a; Thompson 1999; Emmett et al. 2000; Roman et al. 2000; Brock and Chauvaud personal communication; http://chl.wes.army.mil/research/estuaries/lagunamadre; http://hydrography.ims.plym.ac.uk/swamiee/Gironde/swam_genset.html; http://weber.u.Washington.edu/~cretmweb/CRET.html; http://www.edf.fr.cosinus/loire.pdf; http://www.es.flinders.edu.au/~mattom/ShelfCoast/chapter17.html; http://www.shom.fr/fr_page/fr_act_geo/Tpcooper.html; http://www.sfbay.wr.usgs.gov/access/wqdata; http://www.stolt.nl/honfleur; html; http://www.three.state.tx.us/water/quality/data/wmt)samplequery.html

Many models of phytoplankton dynamics do not account for tidal oscillations of surface elevation, and estimates of phytoplankton growth based on field measurements in well-mixed systems usually implement a constant mean water column height. If tidal range is large compared to mean height (especially if $\Delta H^* \gtrsim 0.6$), then tidal shallowing and deepening may significantly influence net phytoplankton growth. In such a case, models or estimates of long-term phytoplankton growth may overestimate or underestimate net growth and could even predict the wrong sign associated with net growth rate, if water surface fluctuations are neglected.

RELEVANCE

The full gamut of phytoplankton growth sensitivity to tidal range covered in Fig. 4 is relevant to real estuaries. In Fig. 7, we show the same α_x^* map

as in Fig. 4 (thus assuming the same physiological and environmental conditions) with points added to represent real estuaries. Average k_t, ΔH and $\overline{H}$ were used to calculate ΔH^* and k_t^* and locate each estuarine region in k_t^*-ΔH^* space. We selected a set of estuaries which demonstrates that the full k_t^*-ΔH^* domain in Fig. 4 includes combinations of physical conditions that occur in the world's estuaries. In the lower left region, the Columbia River, Laguna Madre (Texas), Galveston, Narragansett, and Hudson/Raritan represent systems where turbidity is low and tidal range is small relative to mean water column height. Because α_x^* contours are relatively vertical in that region of the plot, phytoplankton growth in these systems is, on average, relatively insensitive to tidal oscillations in water column height. In the lower right of Fig. 7, the Loire estuary and Bristol Channel are also collocated with relatively vertical iso-α_x^* lines, representing additional systems where phytoplankton growth, on average, is insensitive to tidal range. These are turbid estuaries with a small dimensionless tidal range. We might expect phytoplankton dynamics in these systems to be sensitive to tidal shallowing and deepening because their tidal range is relatively large, but model results suggest that the ratio of tidal range to mean depth is critical, not the magnitude of tidal range itself. The Bay of Brest is located in the upper left portion of Fig. 7, where α_x^* contours bend to the left. Phytoplankton growth in this shallow, clear, macrotidal system may therefore be sensitive to tidal oscillations in water column height and may decrease with increasing tidal range. The Seine (upstream of Honfleur), Yangtze (mouth bar region), Cordouan Shoals of the Gironde, Tamar (U.K.), and Severn are located in the mid-upper right portion of the plot, where iso-α_x^* lines bend to the right. In these light-limited, relatively shallow, mesotidal to macrotidal environments, phytoplankton growth may be sensitive to tidal shallowing and deepening and may increase with increasing tidal range.

In Fig. 7, most estuarine regions are represented by single points based on average or median conditions. Turbidity, tidal range, and mean water column height vary in space and time, so a real estuary may span different regimes in k_t^*-ΔH^* space. Each estuary, represented for simplicity by a single point in Fig. 7, most likely encompasses a range of k_t^* and ΔH^* and therefore a range of relationships between fluctuating water surface elevation and phytoplankton population growth. Bathymetric variability, as well as changes in ΔH over the spring-neap cycle or across the land-sea gradient and variability in suspended particulate concentrations, can result in significant spatial and/or temporal

variability in the relationship between phytoplankton growth and tidal range within an estuary. Shallow regions of South San Francisco Bay correspond with the upper left portion of Fig. 7, whereas the deep channel corresponds with the lower right region. Since phytoplankton growth sensitivity to tidal range increases as mean water column height decreases, tidal shallowing and deepening may have the greatest influence on phytoplankton growth in shallow regions, where blooms in many estuaries are initiated. Therefore, influence of tidal range on phytoplankton population growth may be strongest where bloom activity is greatest.

We have used a numerical model to show that tidal time-scale physical-biological interactions can strongly influence the dynamics of phytoplankton over the longer (weekly, monthly) time scales characteristic of many sampling programs. Although here we used a particular set of physiological and environmental parameters, the lessons produced from our model simulations are general. Tidal fluctuations in water surface elevation and consequently in the depth-integrated source-sink balance can determine whether phytoplankton biomass increases or decreases over time, especially in a shallow, mesotidal to macrotidal water column with a benthic phytoplankton sink. Phasing of tidal oscillations in surface elevation with the diel cycle of solar irradiance is another hourly-scale mechanism that can govern the long-term trajectory of phytoplankton biomass. Phasing of solar noon and low tide has been previously documented as an important mechanism governing growth cycles of benthic microalgae (Nichols and Thompson 1985); our modeling study illustrates how this phasing can influence phytoplankton dynamics as well. Since the period associated with phasing of the solar irradiance cycle and the semidiurnal tide cycle is close to the spring-neap period, the effects of processes associated with one period could be confused with responses to processes associated with the other. This similarity in periods can produce critical, persistent interactions between the two sets of processes (e.g., spring-neap variability in grazing pressure interacting with the cycle of phased surface irradiance with low tide). The relative phasing of these approximately biweekly-scale interactions can produce a range of phytoplankton growth responses, including an oscillating biweekly growth-decline cycle or persistent near-zero growth.

Chlorophyll measurements in South San Francisco Bay are consistent with the biweekly-scale mechanisms demonstrated by the Zero-D model. The time series in Fig. 8 is a 24-h running mean of chlorophyll fluorescence measurements taken every 30 min at the Port of Redwood City in November 2000. Predicted daily maximum tidal cur-
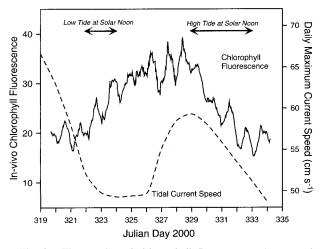
Fig. 8. Time series of chlorophyll fluorescence (measured with a Turner Designs Self-Contained Underwater Fluorescence Apparatus) and predicted daily maximum current velocity in Redwood Creek, South San Francisco Bay, in November 2000. Also noted are periods during which solar noon coincided with low tide and high tide.

rent speed (Foreman 1978) is plotted as well (current speed is low during neap tide and high during spring tide). Also noted are the periods during which solar noon coincided approximately with low tide and high tide. Chlorophyll increased overall during neap tide (when low water and solar noon co-occurred) and decreased during spring tide (when high water and solar noon co-occurred). These measurements are consistent with the model results in Fig. 5.

The local processes studied here constitute only a subset of the forces driving phytoplankton population variability in real estuaries. Local sources and sinks are not typically uniform in the horizontal, and an oscillating tidal velocity field advects phytoplankton across spatial source-sink gradients as those gradients vary in time (Lucas et al. 1999b). Phasing of tidal-scale transport with hourly-scale variations in spatially heterogeneous local processes can determine whether a bloom persists or decays over time. Other high-frequency influences on long-term phytoplankton growth (not addressed here) include pulses of sediment-derived nutrients, tidal and wind-driven resuspension of sediment (May et al. in review), and variations in vertical mixing intensity (Monbet 1992). The large number of mechanisms co-operating in real estuaries is a compelling reason for using simple models; like laboratory experiments, models allow us to isolate and study one or a few processes at a time in a controlled fashion and help us generate new hypotheses for looking at complex real systems in new ways. Outcomes from simple models can also provide useful guidelines for constructing more

complex and comprehensive ecosystem models. In this case, a simple zero-dimensional model defines combinations of environmental conditions in which tidal-scale processes absolutely must be incorporated into estuarine ecosystem models.

Literature Cited

Bannister, T. T. 1974. A general theory of steady state phytoplankton growth in a nutrient saturated mixed layer. *Limnology and Oceanography* 19:13–30.

Casulli, V. 1990a. Numerical simulation of shallow water flow, p. 13–22. *In* G. Gambolati, A. Rinaldo, C. A. Brebbia, W. G. Gray, and G. F. Pinder (eds.). Computational Methods in Surface Water Hydrology. Springer-Verlag, Berlin, Germany.

Casulli, V. 1990b. Semi-implicit finite-difference methods for the two-dimensional shallow water equations. *Journal of Computational Physics* 86:56–74.

Chen, J.-Y., S.-Z. Zhu, Q.-R. Lü, Y. Zhou, and S. He. 1982. Descriptions of the morphology and sedimentary structures of the river mouth bar in the Chang Jiang estuary, p. 667–675. *In* V. S. Kennedy (ed.). Estuarine Comparisons. Academic Press, New York.

Cheng, R. T., V. Casulli, and J. W. Gartner. 1993. Tidal, residual, intertidal mudflat (TRIM) model and its applications to San Francisco Bay, California. *Estuarine, Coastal and Shelf Science* 36:235–280.

Cloern, J. E. 1982. Does the benthos control phytoplankton biomass in South San Francisco Bay? *Marine Ecology Progress Series* 9:191–202.

Cloern, J. E. 1996. Phytoplankton bloom dynamics in coastal ecosystems: A review with some general lessons from sustained investigation of San Francisco Bay, California. *Reviews of Geophysics* 34:127–168.

Cloern, J. E., C. Grenz, and L. V. Lucas. 1995. An empirical model of the phytoplankton chlorophyll:carbon ratio—The conversion factor between productivity and growth rate. *Limnology and Oceanography* 40:1313–1321.

Cloern, J. E., T. M. Powell, and L. M. Huzzey. 1989. Spatial and temporal variability in South San Francisco Bay (USA). II. Temporal changes in salinity, suspended sediments, and phytoplankton biomass and productivity over tidal time scales. *Estuarine, Coastal and Shelf Science* 28:599–613.

Dyer, K. R. 1984. Sedimentation processes in the Bristol Channel/Severn estuary. *Marine Pollution Bulletin* 15:53–57.

Eisma, D. 1998. Intertidal Deposits—River Mouths, Tidal Flats, and Coastal Lagoons. CRC Press, Boca Raton, Florida.

Emmett, R., R. Llansó, J. Newton, R. Thom, M. Hornberger, C. Morgan, C. Levings, A. Copping, and P. Fishman. 2000. Geographic signatures of North American West Coast estuaries. *Estuaries* 23:765–792.

Foreman, M. G. G. 1978. Manual for tidal currents analysis and prediction. PMS Report No. 78-6. Institute of Ocean Sciences, Patricia Bay, Sidney, British Columbia.

GLOVER, R. S. 1984. The Bristol Channel—A case for special treatment. *Marine Pollution Bulletin* 15:37–40.

GROSS, E. S., J. R. KOSEFF, AND S. G. MONISMITH. 1999. Evaluation of advective schemes for estuarine salinity simulations. *Journal of Hydraulic Engineering* 125:32–46.

HUZZEY, L. M., J. E. CLOERN, AND T. M. POWELL. 1990. Episodic changes in lateral transport and phytoplankton distribution in South San Francisco Bay. *Limnology and Oceanography* 35: 472–478.

JOINT, I. R. AND A. J. POMROY. 1981. Primary production in a turbid estuary. *Estuarine, Coastal and Shelf Science* 13:303–316.

KOSEFF, J. R., J. K. HOLEN, S. G. MONISMITH, AND J. E. CLOERN. 1993. Coupled effects of vertical mixing and benthic grazing on phytoplankton populations in shallow, turbid estuaries. *Journal of Marine Research* 51:843–868.

LUCAS, L. V., J. R. KOSEFF, J. E. CLOERN, S. G. MONISMITH, AND J. K. THOMPSON. 1999a. Processes governing phytoplankton blooms in estuaries. I: The local production-loss balance. *Marine Ecology Progress Series* 187:1–15.

LUCAS, L. V., J. R. KOSEFF, S. G. MONISMITH, J. E. CLOERN, AND J. K. THOMPSON. 1999b. Processes governing phytoplankton blooms in estuaries. II: The role of horizontal transport. *Marine Ecology Progress Series* 187:17–30.

MEGARD, R. O. AND T. BERMAN. 1989. Effects of algae on the Secchi transparency of the southeastern Mediterranean Sea. *Limnology and Oceanography* 34:1640–1655.

Ministere de l'Environnement. 1980. Recueil des Observations, Campagnes 1980. Ministere de l'Environnement, Centre National Pour l'Exploitation des Oceans, Reseau National d'Observation de la Qualitie du Milieu Marin, Paris, France.

MONBET, Y. 1992. Control of phytoplankton biomass in estuaries: A comparative analysis of microtidal and macrotidal estuaries. *Estuaries* 15:563–571.

NATIONAL OCEANIC AND ATMOSPHERIC ADMINISTRATION. 1990. Estuaries of the United States, vital statistics of a national resource base. National Oceanic and Atmospheric Administration, National Ocean Service, Rockville, Maryland.

NATIONAL OCEANIC AND ATMOSPHERIC ADMINISTRATION AND UNITED STATES DEPARTMENT OF COMMERCE. 1985. National estuarine inventory, data atlas, Volume 1: Physical and hydrologic characteristics. National Oceanic and Atmospheric Administration, Rockville, Maryland.

NICHOLS, F. H. AND J. K. THOMPSON. 1985. Time scales of change in the San Francisco Bay benthos. *Hydrobiologia* 129:121–138.

PLATT, T., D. F. BIRD, AND S. SATHYENDRANATH. 1991. Critical depth and marine primary production, p. 205–218. *In* Proceedings of the Royal Society of London, Volume 246 of B, Biological Sciences. Harrison and Sons, U.K.

ROMAN, C. T., N. JAWORSKI, F. T. SHORT, S. FINDLAY, AND R. S. WARREN. 2000. Estuaries of the northeastern United States: Habitat and land use signatures. *Estuaries* 23:743–764.

SALOMON, J. C. 1988. Oceanographic characteristics of the Seine estuary, p. 79–88. *In* B. Kjerfve (ed.). Hydrodynamics of Estuaries, Volume II, Estuarine Case Studies. CRC Press, Boca Raton, Florida.

STEPHENS, C. V. 1986. A three-dimensional model for tides and salinity in the Bristol Channel. *Continental Shelf Research* 6:531–560.

THOMPSON, J. K. 1999. The effect of infaunal bivalve grazing on phytoplankton bloom development in South San Francisco Bay. Ph.D. Dissertation, Stanford University, Palo Alto, California.

UNCLES, R. J. 1982. Residual currents in the Severn estuary and their effects on dispersion. *Oceanologica Acta* 5:403–410.

UNCLES, R. J., M. B. JORDAN, AND A. H. TAYLOR. 1986. Temporal variability of elevations, currents, and salinity in a well-mixed estuary, p. 103–122. *In* D. A. Wolfe (ed.), Estuarine Variability. Academic Press, San Diego, California.

SOURCES OF UNPUBLISHED MATERIALS

BROCK, D. personal communication. Texas Water Development Board, 1700 North Congress Avenue, P. O. Box 13231, Austin, Texas 78711–3231.

CHAUVURD, L. personal communication. Chargé de Recherche au CNRS, Université de Bretagne Occidentale, Institut Universitaire Européen de la Mer, UMR CNRS 6539-LEMAR, Technopole Brest Iroise, Place Nicolas Copernic, 29280 Plouzané, France.

MAY, C. L., J. R. KOSEFF, L. V. LUCAS, J. E. CLOERN, AND D. H. SCHOELLHAMER. In review. Effects of spatial and temporal variability of turbidity on phytoplankton blooms. *Marine Ecology Progress Series*.